SCIENCEFORECAST
Connecting Research to Drive Scientific Innovation

Research Article
Published: 08 Jun, 2018

SF Journal of Nanochemistry and Nanotechnology

Low Cost Mass Manufacturable Silicon Nano-Sensors for Detection of Molecules in Gas Phase

Hakim MMA[1,2], Tanzeem S[1], Sun K[2] and Ashburn P[2]*

[1]Department of Electrical & Electronic Engineering, East West University, Dhaka, Bangladesh

[2]Nanoelectronics and Nanotechnology Group, University of Southampton, Southampton, UK

Abstract

We report uniform and reproducible thin film polycrystalline silicon (polysilicon) nanowire sensor platform realized by an advanced spacer etch process in a mature 3 micron lithography for room temperature detection of molecules in gas phase. The main strength of the technology is that it is capable of producing polysilicon nanowires with perfectly rectangular shape and reasonably smooth surface in a novel spacer etch process using low density plasma of SF_6 and O_2 gases from a thin film of amorphous silicon (α-Si) layer. The conductance of the realized nano sensors scales reasonably well with nanowire number and length and the measured electrical performance is found to be in reasonable agreement with the design. The conductance variation of randomly distributed nano-sensors in a 6 inch wafer is found to be less than 7% implying a well controlled fabrication process. Comparative measurements in air, vacuum, hydrogen and isopropyl alcohol and 3D numerical simulation on the evolution of surface states of nanowires upon exposure into different gas ambient unequivocally demonstrate the potential of polysilicon nanowires for detecting molecules in gas phase at room temperature with the promising gas sensitivity and impressive response/recovery times. The nano-sensors are developed in a relatively cheap reactive ion etching system using a low density plasma based special etch that provides high quality polysilicon nanowire sensors with excellent uniformity and reproducibility for a simple, low cost, manufacturable route to gas-sensor fabrication.

Keywords: Nanowires; Sensors; Biosensors; Nanodevices; Thin films

OPEN ACCESS

Correspondence:
Hakim MMA, Department of Electrical & Electronic Engineering, East West University, Dhaka-1212, Bangladesh Nanoelectronics and Nanotechnology Group, University of Southampton, Southampton, SO17 1BJ, UK.
E-mail: *dmmah@ewubd.edu*

Received Date: *03 May 2018*
Accepted Date: *04 Jun 2018*
Published Date: *08 Jun 2018*

Citation: *Hakim MMA, Tanzeem S, Sun K, Ashburn P. Low Cost Mass Manufacturable Silicon Nano-Sensors for Detection of Molecules in Gas Phase. SF J Nanochem Nanotechnol. 2018; 1(1): 1006.*

ISSN 2643-8135

Copyright *© 2018 Hakim MMA. This is an open access article distributed under the Creative Commons Attribution License, which permits unrestricted use, distribution, and reproduction in any medium, provided the original work is properly cited.*

Introduction

In recent years, nanowire (NW) based ultrasensitive sensors have been widely investigated for the potential of real time, high sensitivity and label-free detection [1-6]. The driving force towards the development of nanowire based sensors is large surface to volume ratio, and also that one or more of the physical dimensions are less than or comparable to the charge screening length, i.e. the Debye length. As a result, electric field modulation by immobilization of biological or chemical species on the surface affects carrier concentration across the entire cross sectional conduction pathway [2] and hence, NW devices give extraordinary sensitivity [3-5].

Among different nanomaterials, silicon nanowires have the potential advantage of compatibility with very large scale integration (VLSI) and complementary metal oxide semiconductor (CMOS) technologies [7]. These benefits are some of the main reasons for the significant interest in silicon nanowire based sensors with quite a large number of studies on the detection of analytes in aqueous environment, mainly within the context of biosensing (e.g., to detect biological species like DNA, proteins and viruses etc.) and only a few number of studies appearing for sensing in gas phase for workplace safety, environmental pollution monitoring and for the development of novel, non-invasive diagnostics for human healthcare [8]. However, commercial silicon NW based sensors are still unavailable for analyte detection even in aqueous environment due to the difficulty in device manufacturing processes, reproducible sensing/integration issues and most importantly due to the unavailability of economically viable route for mass fabrication. Therefore, the development of a simple and cheap route for nanowire sensor fabrication is needed which may enable mass manufacture of nanowire sensors for personalized, pro-active and preventive healthcare.

Nanowire sensors can be fabricated either using top-down or bottom-up approaches. Bottom-up approaches are capable of producing high quality single-crystal nanowires through metal assisted catalytic process [6], which is simple and cheap. However, nanowire grown using this process is not location controlled and hence, additional non-CMOS post processing steps like

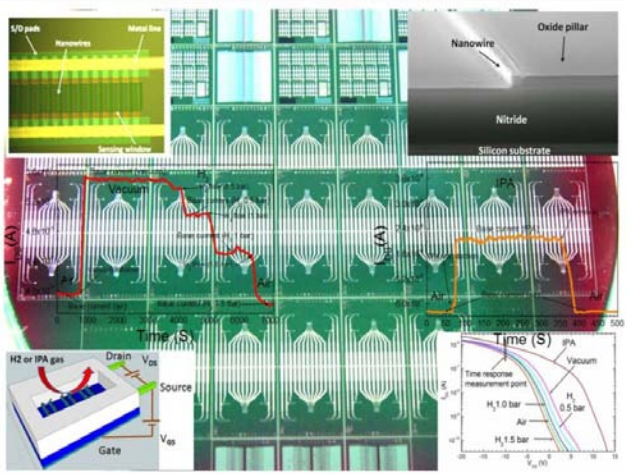

Scheme 1: Plastic substrate compatible thin film slicon nano-sensors and molecule detection in gas phase.

electric field or fluid flow-assisted nanowire positioning is required for electrodes definition making construction of functional device arrays challenging [9]. Additional issues are metal contamination and less control of structural parameters resulting in the poor device uniformity and reproducible integration remains problematic. These shortcomings are eliminated in top down approaches and nanopatterning techniques like deep-UV [10] and electron-beam [11,12] lithography have been used the past to fabricate single crystal silicon nanowires. These techniques provide the advantages of the high density integration possibilities related to the well known CMOS processes, but have disadvantage of elevated budget associated with these advanced lithography techniques and costly SOI wafers. Si NW arrays have also been fabricated using nanoimprint lithography [13], however, fabrication of the master replication stamp is not straightforward due to the requirement of advanced lithography and wafer-level patterning is challenging. To avoid expensive lithography, silicon nanoribbon fabrication by conventional lithography and subsequent thinning by oxidation [14], specialized wet etch [15], wet etch-transfer [16] techniques have been reported which are time consuming and hard to control across a large wafer area. As such the best approach for Si NW fabrication is unclear at present time and a phenomenological development is needed for a commercial scale production [17].

Most recently, a low cost nanowire fabrication technology has been reported which uses spacer etch process on a deposited thin film [18-20]. This technology has attractive feature of defining polysilicon nanowires with nano-scale dimensions using mature lithography and industry standard deposition and spacer etch techniques. This process also enables the use of glass or plastic substrates which could open up opportunities in low cost disposable diagnostics and in portable, wearable or even implantable sensors. However, the main challenge in this technology is that the realized nanowires are approximately quarter circle shaped as during dry etch of nanowires no mask protection is used and hence, the corner of the nanowire is affected by the plasma [19-22]. This makes control of the nanowire volume across a wafer challenging and hence, manufacturability of the process could be severely affected by degraded uniformity and reproducibility in characteristics. Dry etch processes are also susceptible to the creation of interface states due to etch damage which may significantly affect the NW sensitivity by favouring charge trapping at the Si/SiO_2 interface [15], degraded leakage [23] and sub-threshold characteristics [24] thereby affecting the NW's capability to react efficiently to the manipulation of the gate (or molecular gating) voltage. In fact, plausible uniformity in the nanowire characteristics and economic feasibility of the nanowire realization process are some of the key challenges for the commercial availability of nanowire based devices in near future. We have previously demonstrated the potential of polysilicon nanowires for detecting the proteins interleukin-8 (IL-8) and tumor necrosis factor-alpha (TNF-α) in aqueous environment and have validated nano-sensors against standard enzyme-linked immunosorbent assays (ELISAs) [25]. However, the detection of molecules in gas phase using polycrystalline silicon nanowires and theoretical study to gain physical understanding on the evolution of surface charges of nanowires upon exposure of different gas ambient are rare in the literature. A study of the wafer scale uniformity/reproducibility; width, shape and surface morphology control of polycrystalline silicon nanowires prepared by spacer etch process is also not available in the literature.

This article first time performs a quantitative evaluation of the uniformity and reproducibility of the thin film polycrystalline silicon nanowire sensors and investigates the performance of the nanowires in various gases with a view to gas sensing applications. Perfectly rectangular and reasonably smooth polycrystalline silicon (polysilicon) nanowires are realized by mature 3 micron lithography and spacer etch using low density plasma of SF_6/O_2 gases in low cost reactive ion etch (RIE) equipment and, delivering appreciable control of the nanowire width and shape across a 6 inch wafer. Comparative measurements in air, vacuum, hydrogen and isopropyl alcohol are conducted to demonstrate the nano-sensor's capability to detect molecules in the gas phase. In addition, ambient effects on the nano-sensor conductance are studied for the first time using 3D numerical simulations to gain physical understanding on the evolution of surface charges of the polysilicon nanowires upon exposure of different gas ambient.

Experimental

The sensor fabrication started with the deposition of 500nm nitride and 100nm oxide layers on (100)-oriented n-type silicon wafers with a doping of $10^{16}/cm^3$ using plasma enhanced chemical vapour deposition (PECVD) (Figure 1a). A photolithography step was done using mature microelectronics lithography (line width > 3μm) and the 100nm oxide layer was dry etched anisotropically to create oxide pillars (Figure 1a). After resist strip and cleaning a 100nm undoped LPCVD amorphous silicon (α-Si) film was deposited using the pyrolysis of silane at 560°C and subsequently doped by boron implantation at a dose of $1.5\times10^{13}/cm^2$ and an energy of 25keV (Figure 1b). Another photolithography step was again done and source/drain pad regions are implanted by boron at a dose of $4\times10^{15}/cm^2$ and an energy of 35keV (Figure 1b). This α-Si film was dry etched using low density plasma with 12sccm SF_6 and 12sccm O_2 at a pressure of 30mT, a reactive ion etching (RIE) power of 160W, and a plate temperature of 20°C in an Oxford Instruments capacitively coupled RIE system. The etch leaves amorphous silicon spacers (nanowires) around the oxide pillar sidewalls, while source/drain pad regions are protected from etch by photoresist (Figure 1c). After resist stripping a 10nm gate oxide was grown at 900°C which crystallised the amorphous silicon to polycrystalline silicon and activated the implanted dopant. Aluminium contacts were realised on the heavily doped source/drain pads to either end of the polysilicon nanowire (Figure 1d).

Table 1: The conductance ratio of NWs with different lengths with the conductance of 14μm long NW. Measured NW blocks have 60NWs connected in parallel.

Substrate voltage (V_{GS})	The conductance ratio of NWs with different lengths with the conductance of 14μm long NW			
	24 μm	36 μm	48 μm	58 μm
0	1.45	2.43	3.21	4.48
-5	1.6	2.35	3.32	4.62
-10	1.41	2.28	3.24	4.56
-15	1.46	2.25	3.16	4.34
-20	1.47	2.27	3.25	4.21
-25	1.55	2.31	3.31	4.43

Table 2: The conductance ratio of NWs for different numbers of NWs connected in parallel with the conductance of 10NWs connected in parallel. The NWs have the length of 14μm.

Substrate voltage (V_{GS})	The conductance ratio of NWs for different numbers of NWs connected in parallel with the conductance of 10 NWs connected in parallel					
	20	40	60	80	100	160
0	1.81	3.88	6	7.82	10.51	15.86
-5	1.93	3.8	6.23	7.83	10.84	15.8
-10	1.89	3.91	6.14	7.92	11.06	16.27
-15	1.83	3.88	6.41	7.89	11.05	15.9
-20	1.9	3.91	5.99	7.91	10.66	15.79
-25	1.88	4	6.06	8	10.97	15.94

An insulator layer was then deposited and subsequently a sensing window was opened over the nanowires for effective passivation of contacts from sensing regions (Figure 1e). Such a passivation scheme provided the flexibility of testing nanowire sensors both in aqueous environment and in different gases without any effect on metal-semiconductor contacts in source/drain regions. The physical structure of the nanowires (width, shape and surface morphology) was investigated by plan-view and cross-sectional scanning electron microscopy (SEM) and Nomarski Differential Interference Contrast (DIC) Microscopy. Figure 2 shows a wafer map of the completed nano-sensors consisting of 39 nano-sensor chips with numbers of test structures for characterising etch uniformity across the wafer. Each chip consists of eight nano-sensors where the outer nano-sensors comprise 30 nanowires connected in parallel, each with a length of 48μm. The inner nano-sensors have different nanowire lengths and/or nanowire numbers connected in parallel. Electrical characterisation of the nano-sensors was performed using an Agilent B1500A Semiconductor Parameter Analyser. The gas sensing measurements were performed utilizing the sealed chamber of a Lakeshore EMTTP4 probe station which was connected to a H_2 gas cylinder with a pressure control valve. Simulations were performed using a SILVACO TCAD Tool.

Results

Width and shape of nanowires after spacer etch

Figure 3a shows a cross-sectional Scanning Electron Microscopic (SEM) image of the nanowire. The nanowires are rectangular in shape with measured width and height of 95nm × 95nm. This provides a good basis for reproducible control of the nanowire shape. Figure 3b shows a plan view SEM image and indicates that the nanowire is continuous, with a reasonably uniform width. To quantify the etch uniformity, the nanowire width has been measured from high magnification plan-view SEM images in 20 different locations on a wafer and values of mean and standard deviation are calculated. The mean and standard deviation of width are found to be 95nm and 4nm respectively while the original α-Si layer was 100nm thick. This result indicates that the SF_6/O_2 plasma etch process is highly anisotropic and therefore gives good control of the nanowire width. To further quantify the etch uniformity, cross sectional SEM images were captured from the test structures located at regions A, B and C of Figure 2a. It is observed that the perfectly rectangular shape of the polysilicon nanowires and its dimensions are well maintained across the 6 inch wafer. This confirms the uniformity of the SF_6/O_2 plasma etch. It is worth mentioning that reported polysilicon nanowires prepared by spacer etch generally exhibit a roughly quarter circle shape with pronounced etching in the horizontal direction indicating the loss of anisotropy [19-22] (inset of Figure 3a). In addition, sidewall striations and random accumulation of polymers are often observed due to incomplete removal of passivation layers [26-27]. In this regard, the SF_6/O_2 plasma etch is better suited to nanowire fabrication than alternative etches. Details of the etch uniformity investigation are provided in the supplementary information.

Electrical characteristics

We now investigate the electrical characteristics of the fabricated nanowires. Figure 4a shows output characteristics of 14μm long polysilicon nanowires for different substrate voltages (V_{GS}). The characteristic exhibits typical transistor like behaviour where nanowire conductance is significantly affected by substrate bias voltage. The I_{DS} value at V_{DS}=4V increases from 0.34nA at V_{GS}=0V to 0.28μA at V_{GS}=-25V. Figure 4b shows typical transfer characteristics of nanowire measured for different values of drain to source voltages (V_{DS}). The characteristic exhibits a sub-threshold slope around 2.3 to 3.0 V/decade while substrate has been used as gate and 500nm nitride has been used as gate insulator. Activated doping concentration of nanowire predominantly controls its sensitivity as a sensor and this phenomenon is drastically different for single-crystal and polycrystalline silicon nanowires for a same implant dose. The implanted boron dose of $1.5\times10^{13}/cm^2$ should deliver to deliver a doping concentration around $1\times10^{18}cm^{-3}$ in single-crystal silicon nanowires as it is expected that all of the implanted dopants are electrically activated by activation anneal. However, doping

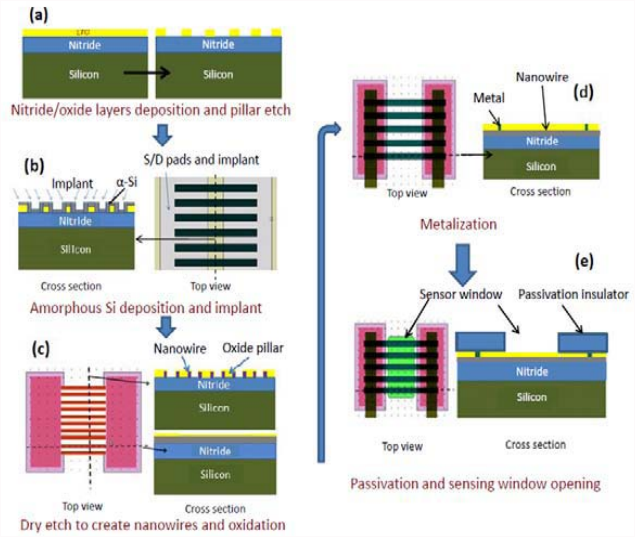

Figure 1: Schematic process flow of the polysilicon nanowire sensor fabrication.

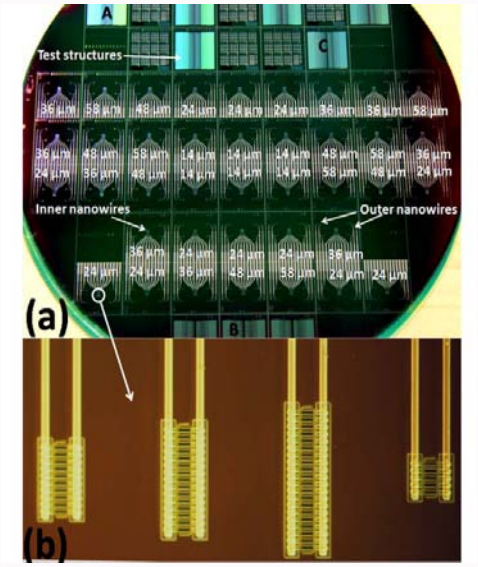

Figure 2: Wafer map of the completed nano-sesnor wafer fabricated using low density plasma of SF_6 and O_2 gases in a cheap reactive ion etch (RIE) equipment consisting of nano-sensor chips and test structures.

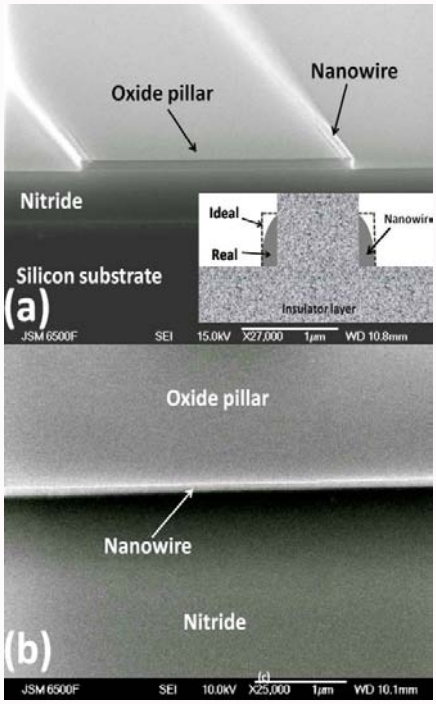

Figure 3: a) Cross-sectional and b) Plan view Scanning Electron Microscopic (SEM) image of the nanowire defined from a thin film of α-Si layer deposited on a prior fabricated oxide pillar using low density plasma based shallow etch with a simultaneous flow of etchant SF_6 and inhibitor O_2 in a cheap capacitively coupled reactive ion etch (RIE) equipment.

segregation at grain boundaries may capture some of the implanted dopants for polysilicon nanowires and hence the electrically active doping concentration may be lower than the expected doping of $1\times10^{18}cm^{-3}$. To investigate this phenomenon, we have calculated active hole concentration in our fabricated polysilicon nanowire using the method described in our previous report [25]. It is found that the active hole concentration is around $2\times10^{16}cm^{-3}$ for a bias voltage of V_{GS}=-5V and V_{DS}=0.5V, which is reduced to value of $7\times10^{15}cm^{-3}$ at V_{GS}=0V and V_{DS}=0.5V. This value of hole concentration indicates electrically active doping concentration of polyslicon nanowires which is noticeably lower that the expected doping concentration of single-crystal silicon nanowires ($1\times10^{18}cm^{-3}$), thereby explaining very low conduction in our nanowires.

To investigate the uniformity of the nano-sensors, Figure 5a shows nanowire conductance as a function of nanowire length for different substrate voltages (V_{GS}). The measurements were performed on-sensor blocks at different location on the wafer which vary from one another in nanowire lengths as shown in Figure 2a. It can be seen that the conductance increases with decreasing substrate bias. The nano-sensor block with nanowire length of 14μm exhibits a conductance of 1.5 $\times10^{-2}$μS at V_{GS}=0V which increases to a value of 2.5μS at V_{GS}=-25 V. The conductance increase of p-type polyslicon NWs with negative substrate voltages (V_{GS}) can be explained by the significant hole accumulation in the NW body upon application of the negative V_{GS} voltages. However, it is interesting to note that the NW conductance decreases almost linearly with increasing NW lengths at long nanowires whereas a mild non-linearity can be observed at short nanowires due to the heavily doped contact pad/associated aluminium contact resistances which affects the measurement at short NW lengths. However, the conductance ratio of NWs with different lengths with the conductance of 14 μm long NW is presented in Table 1. The exhibited conductance ratio of NWs are in reasonable agreement with ideal values of 1.7, 2.6, 3.4 and 4.1 for 24, 36, 48 and 58 μm long nanowires at all substrate voltages (VGS). Figure 5b shows nanowire conductance as a function of the number of parallel nanowires for various values of substrate voltage (V_{GS}). It is observed that the NW conductance increases linearly with increasing numbers of NWs connected in parallel for all substrate voltages (V_{GS}). The conductance ratio of NWs for different numbers of NWs connected in parallel with the conductance of 10NWs connected in parallel is presented in Table 2. The exhibited conductance ratio is again found to be in reasonable agreement with expected values of 2, 4, 6, 8, 10 and 16 for 20, 40, 60, 80, 100 and 160 numbers of NWs connected in parallel at all substrate voltages (V_{GS}).

To investigate the uniformity of the nano-sensors further, Figure 6 shows output characteristics of several 48μm long nano-sensor

Table 3: Comparison of the gas sensing figure of merit (i.e. conductance change, response/recovery times) of fabricated polysilicon nanowire sensors with the reported pristine silicon based sensors for the detection of H_2 and polar volatile organic compound (i.e. IPA).

Si NW size	Type/approach	Target	Conductance change	Response time	Recovery time	Ref.
Inorganic gas						
NA	Porous single crystal Si	H_2	18% at 5% H_2	-	-	47
			50% at 10% H_2	-	-	
d = 300nm L = 5.25µm	Single crystal Si NW synthesized by metal assisted chemical etch	H_2	60% at pure H_2	180 seconds	No recovery	48
d = 95nm L = 58µm	**Poly silicon nanowire by spacer etch (This work)**	**H_2**	**5% H_2 in air**	**100-120 seconds**	**101 seconds**	**This work**
			16% at 0.5 bar 32% at 1.0 bar 65% at 1.5 bar			
			5% H_2 in vacuum			
			70% at 0.5 bar 90% at 1.0 bar 97% at 1.5 bar			
Polar volatile organic compounds						
d = 30 to 70 nm L = 400nm to 1µm	Top down/bottom up grown single crystal Si NWs	Polar VOC (Methanol, Ethanol, Isopropanol)	50%	40 seconds	50 seconds	45
d = 95nm L = 58µm	**Poly silicon nanowire by spacer etch (This work)**	**Polar VOC (IPA)**	**3.6 × 10⁵%**	**15 seconds**	**32 seconds**	**This work**

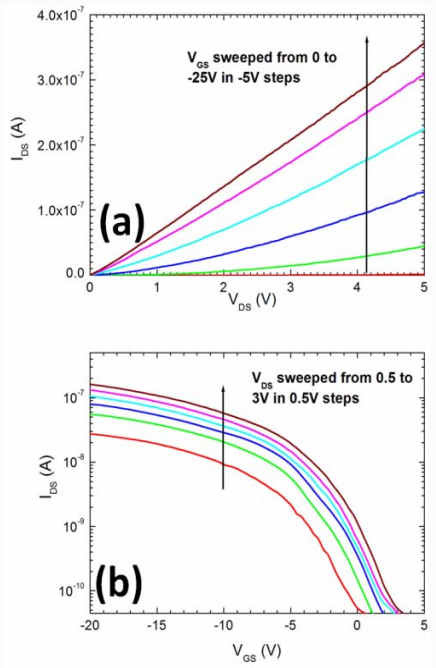

Figure 4: Polysilicon nanowire electrical characterisation; a) Polysilicon nanowire output characteristic (I_{DS} as a function of V_{DS} for different V_{GS} values); b) Polysilicon nanowire transfer characteristic (I_{DS} as a function of V_{GS} for different V_{DS} values). The nanowire has a length of 14 µm and during this measurement wafer substrate is used as gate with 500nm nitride as gate insulator.

blocks at different substrate voltages (V_{GS}). The nano-sensor blocks have 30 nanowires connected in parallel and are chosen from five different places on a 6 inch wafer (left, right, bottom and middle of Figure 2a). The drive current increases with decreasing V_{GS} and the average currents are 0.034±1.1%, 0.15±5.25%, 0.62±3.97%, 1.13±3.7%, 2.23±6.41% and 4.53±6.65% µA at V_{GS} values of 0, -5, -10, -15, -20 and -25 V and for V_{DS} equal to 5V. The standard deviation of drive current lies within the range 1% to 7%, thereby demonstrating that the SF_6 and O_2 plasma etch process is reasonably uniform.

Gas sensing

To demonstrate the nano-sensor's capability to detect molecules in gas phase and/or to elucidate the effects of the surrounding ambient on the NW conductance, measurements were made in different gases. This measurent is done using a nano-sensor block which comprises 58µm long nanowires and 30 nanowires connected in parallel. Figure 7a shows the measured current sequentially in air, vacuum and H_2 (5%) gases at different pressures as a function of time for bias voltages of V_{DS}=5V and V_{GS}=-10V. It is observed that the nano-sensor current changes systematically as the gases are changed. It increases by 45% when the ambient is changed from air to vacuum with a response time (time taken to reach 90% of the equilibrium value) of 101 seconds. In contrast, the change of ambient from vacuum to H_2 leads to a decrease in NW current. Sequential flow of H_2 pressures 0.5, 1.0 and 1.5 bar give decreases in NW current of 13%, 10% and 16% from the base current level with response times of 100, 127 and 120 seconds. Figure 7b shows the time response of the NW current for Isopropyl Alcohol (IPA). This investigation is done on the same nano-sensor chip that is used in the previous measurement and the NWs are exposed to IPA vapor by applying a drop of the solvent (5µl) to a tissue above a hole in a measurement box. Notably the current is steeply increases by 450% from the low base current around 417nA in air when the NW is exposed to IPA vapour. The response time of NW to IPA vapour is found to be 15 seconds. The nanowire current recovered to the value in air when the IPA vapour source was removed with a recovery time around 32 seconds.

Figure 8a illustrates typical transfer characteristics of NW using substrate as gate and 500nm nitride as gate insulator measured alternately in air, vacuum, IPA and in H_2 gases at different pressures. This measurement was performed on the same nano-sensor chip that was used for time response measurement presented in Figure 7. Some noticeable changes in the sub-threshold characteristics can be observed when the nano-sensor chip was exposed into different gas ambient. Exposure into air, vacuum, H_2 gases with different pressures and IPA do not significantly changes sub-threshold slope of the nanowires with a value around 2.6V/dec whereas a significant shift of the sub-threshold characteristic is observed with the change of the

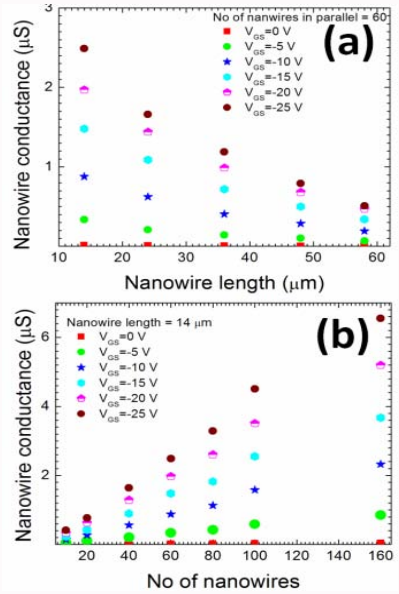

Figure 5: Nanowire conductance as a function of a) Nanowire length and b) Numbers of nanowires connected in parallel at different substrate voltages (V_{GS}). The measurements were performed on-sensors at different location on the wafer which vary from one another in nanowire lengths and nanowire numbers connected in parallel.

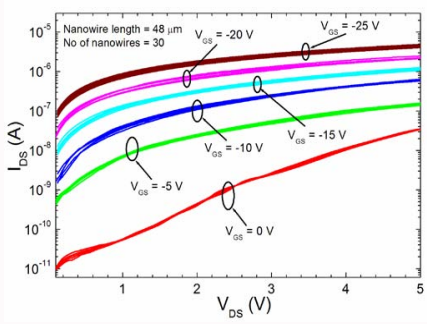

Figure 6: Output characteristics of 48μm long nano-sensor blocks at different substrate voltages (V_{GS}). The nano-sensor blocks have 30 nanowires connected in parallel and are chosen from five different places on a 6 inch wafer (left, right, bottom and middle of Figure 1a).

surrounding ambient. This shift is quantified using constant current threshold method at a current level of 4×10^{-8}A which is just below the knee of sub-threshold curve. The ambient change from air to vacuum exhibited a positive threshold voltage shift (ΔV_{TH}) of 2.47V whereas the ambient change from vacuum to H_2 gas exhibited negative ΔV_{TH} shift with values of -1.14V, -2.09V and -3.16V respectively for H_2 gases with pressures of 0.5, 1.0 and 1.5 bar. The transfer characteristic of the nano-sensor in IPA ambient is quite distinct with a significant positive ΔV_{TH} of 10.48V with respect to air. Figure 8a also demonstrate that the nanowire's conductance change due to ambient change from air to vacuum, air to IPA and vacuum to H_2 gas strongly depends on the substrate voltage (V_{GS}). The chosen V_{GS}=-10 V for time response measurement presented in Figure 7 is in saturation region of the characteristics and exhibited conductance changes are low when nanowires' ambient is changed. However, Figure 8b shows the nanowire conductance change (%) as a function of substrate voltage (V_{GS}) when the ambient is changed from air to vacuum, air to IPA and vacuum to H_2 gases with different pressures. As can be seen from the Figure 8b, our polysilicon nanowire sensors demonstrate a phenomenological response when the operating point is within the linear region of the sub-threshold regime with peak conductance changes of 1560%, 3.6 × 105%, 70%, 90% and 97% when the ambient is changed from air to vacuum, air to IPA and vacuum to H_2 gases with different pressures respectively. These results unambiguously demonstrate the potential of poly silicon NWs as high sensitivity gas sensors at room temperature.

Discussion

Spacer etch has been extensively used in CMOS process line for creating nitride spacers prior to silicidation [28] and recently it has been used for polysilicon nanowire definition [18-22]. Anisotropic etching of silicon is typically achieved by sidewall passivation based etching techniques [27,29-31] where directional etching is achieved by inhibiting the isotropic chemical etch in lateral direction by coating trench sidewall with polymers. Usually high density plasma associated elevated chemical reaction makes the isotropic tendency of chemical etch difficult to control and an incomplete removal of passivation component within the brief etch time required to process thin film of α-Si layer [29-31]. This results in either the quarter circle shape of NW or the formation of grass-like residues and pile-up of excess polymers. In our spacer etch, the control of plasma density and hence, the control of the isotropic tendency of chemical etch is achieved by 4 times reduction of etchant SF_6 and the control of the deposition/removal of passivation polymer is achieved within the brief etch time required to process thin film of α-Si layer by 8 times reduction inhibitor O_2 flow rate in the system in comparison to standard spacer etch process [29-31]. Figure 3 shows that such a mechanism of low density SF_6/O_2 plasma on thin film of α-Si layer delivered nanowires with ideal rectangular shape with hardly visible sidewall striations and/or polymer particles or glass-like residues. The perfectly rectangular shape and reasonably smooth surface of polysilicon nanowire thus maintained across the 6 inch wafer and the electrical outcome is quite promising. A reasonable agreement of nanowire conductance with nanowire numbers and nanowire lengths is achieved (Figure 5) and a less than 7% conductance variation of randomly distributed nanowires across a 6 inch wafer is found (Figure 6). Previous reports suggest that size effects on nanowire transport and conductance are highly anomalous [32]. This has been attributed to the dominant surface charge effects due to the high surface to volume ratio of nanowire and to the nanowire dimension or doping variations due to the random fluctuation in the growth or etching process [32-35]. However, our results show that the low density SF_6 and O_2 plasma based RIE process is quite successful in maintaining uniformity of nanowire dimensions and its inherent properties across a 6 inch wafer while the process is inherently cheap.

Figure 7 and 8 show that fabricated polysilicon nanowire sensors are extremely sensitive to ambient, H_2, volatile IPA gases and it is worth noting that the NW conductance noticeably increases when the ambient is changed from air into vacuum. It has been reported that adsorption of gas molecules from atmosphere traps carriers which significantly influences the electrical properties of semiconductor nanostructures [36-37]. However, the effect of these surface charges on the conduction properties of nanowires is found to be inherently process dependent [15,32,38]. Jie et al. [32] observed a reduction of nanowire conductance in synthesized p-type silicon nanowires when the ambient is switched from air to vacuum. This was explained by adsorbed water molecules forming OH^- ions thereby causing accumulation of excess holes in nanowire and an enhancement of the conductance in air. In contrast, etched Si nanowires exhibited

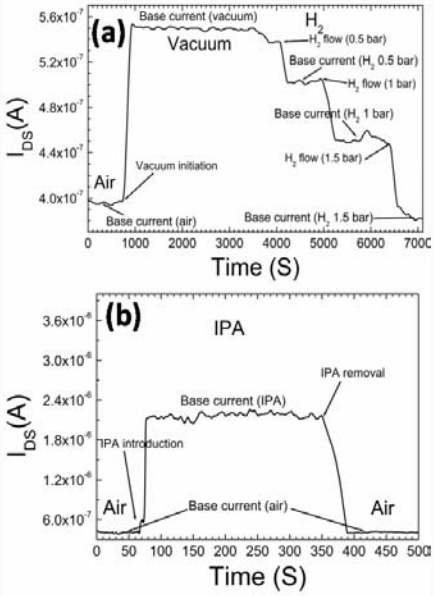

Figure 7: Time dependence of nano-sensor current I_{DS} when the sensor was exposed a) To air, vacuum and in H_2 gases with different pressures and b) To vapours of IPA. For this measurement a nano-sensor block is chosen which have 58 µm long nanowires and 30 nanowires connected in parallel. The nano-sensor is supplied with bias voltages of V_{DS} = 5V and V_{GS}= -10 V.

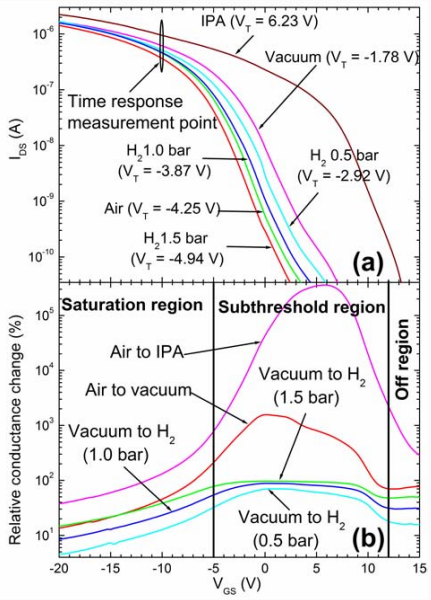

Figure 8: a) Sub-threshold characteristics of nano-sensor using substrate as gate and 500nm nitride as gate insulator measured alternately in air, vacuum, IPA and in H_2 gases with different pressures and b) nano-sensor's conductance change (%) as a function of substrate voltage (V_{GS}) when the ambient is switched from air to vacuum, air to IPA and vacuum to H_2 gases with different pressures. This measurement is performed on the same nano-sensor chip that was used for time response measurement presented in Figure 7. The nano-sensor block has 58µm long nanowires and 30 nanowires connected in parallel.

that original conductivity of silicon wafer is not inherited in nanowires and p-type silicon nanowires showed significantly reduced conductivity due to surface charge associated depletion [15]. Fujii et al. [38] observed conductance increase in p-type air bridged structured silicon nanowires in vacuum that was prepared by dry etch. Our results resemble etched silicon nanowires reported by Chen et al. [15] and Fujii et al. [38] and a reduced conductivity is observed due to surface charge associated depletion in air. However, these surface charges are related to air and switching the ambient from air into vacuum is found to reduce the effects of these surface charges thereby increasing nanowire conductance in vacuum. Although the exact constituents of these surface charges cannot be identified it can be decided that these atmosphere dependent surface charges are most likely donor type which has the characteristics of depleting p-type nanowires by locally accumulating positive charges at the nanowire surface in air.

To further investigate the nature of surface/interface states of fabricated polysilicon nanowires in air, a 3D simulation of electrical characteristics of p-type polysilicon nanowires is done by creating a 14µm long, 95nm × 95nm polysilicon nanowire on 500nm nitride and a n-type silicon substrate with a doping of $10^{16}/cm^3$ in SILVACO TCAD platform. As fabricated, the NW is covered with 10nm oxide layers and source/drain contacts are connected through a heavily doped p-type silicon layer with doping density of $10^{20}/cm^3$. To accurately model the characteristics of the nanowire, a continuous trap states (both donor-like and acceptor-like) distribution across the energy band gap is used for polysilicon material with parameters previously used in the literature for successful modelling of polyslicon thin film transistors [39]. For surface states, acceptor or donor type states with varying densities are invoked both in the top oxide/polysilicon and bottom nitride/polysilicon interface and tested. Donor-like and acceptor-like tail states, Gaussian distribution of mid gap states inside polysilicon nanowire and different types of surface states affect the electrical characteristics of p-type polysilicon nanowires quite a different manner, the details of which is out of the scope of the current manuscript and will be reported elsewhere. However, Figure 9a compares the simulated and measured transfer characteristics (I_{DS} as a function of V_{GS} for V_{DS} value of 0.5V) of the 14µm long nanowire with different densities of acceptor like states. As can be seen from Figure 9a, reported continuous distribution of polysilicon defect states [39] and acceptor like surface states fail to reproduce electrical characteristics of our polysilicon nanowires in air. Acceptor like surface states only affects leakage current of p-type polysilicon nanowire at the positive V_{GS} regime. Figure 9b compares the simulated and measured transfer characteristics of the 14µm long nanowire with different densities of donor like states. It is observed that donor type states affect polysilicon nanowire's sub-threshold and on current characteristics. Donor like states are located at the lower half of the band gap whereas acceptor like states is located at the upper half of the band gap. As a result, depending on the position of the Fermi level which depends on VGS, donor like and acceptor like states show different behaviour in different operation regime.

Figure 10a compares the simulated and measured transfer characteristics (I_{DS} as a function of V_{GS}) for different V_{DS} values for the 14µm long nano-sensor block and it is found that donor type surface states with a density of $1.6\times10^{11}/cm^2$ is quite successful to reproduce the measured sub-threshold characteristics of 14µm long nanowires in air at all V_{DS} voltages. This implies that the surface states of the fabricated polysilicon nanowires excluding grain boundary defects is around ~$10^{11}/cm^2$ which is similar to the synthesized single crystal silicon nanowires reported by Jie et al ($4.3\times10^{11}/cm^2$) [32] and consistent with the observed surface charge densities of silicon (~$10^{12}/cm^2$) [40]. It is worth mentioning that single crystal silicon nanowire

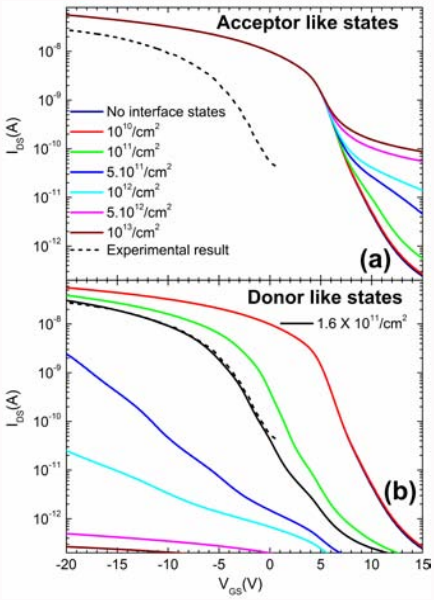

Figure 9: Comparison of the simulated and measured transfer characteristics (I_{DS} as a function of V_{GS} for V_{DS} value of 0.5V) in air for a nano-sensor block with different densities of: a) Acceptor likes states and b) Donor like states. The sensor block has a nanowire length of 14µm and during this measurement/simulation wafer substrate is used as gate with 500nm nitride as gate insulator.

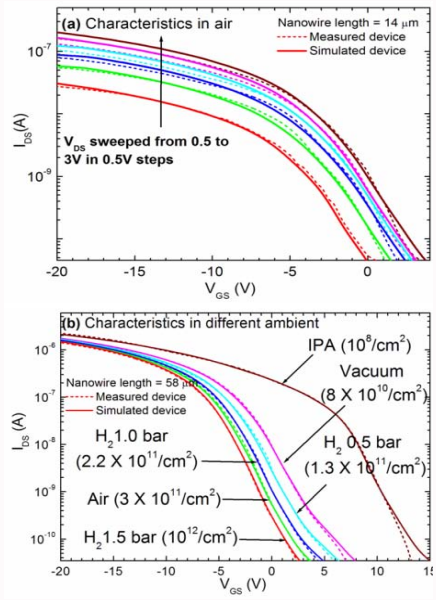

Figure 10: a) Comparison of simulated and measured transfer characteristics (I_{DS} as a function of V_{GS} for different V_{DS} values) of nano-sensor in air which comprises 14µm long nano-wire and b) Comparison of the simulated transfer characteristics (I_{DS} as a function of V_{GS}) of the 58µm long nanowires with different densities of surface states with the measured sub-threshold characteristics of the nano-sensor block with 58µm long nanowires in different gas ambient. During this measurement wafer substrate is used as gate with 500nm nitride as gate insulator.

with a growth direction can have a density of dangling bonds as high as $10^{15}/cm^2$ [32]. To discuss the response of polysilicon nanowires in H_2 and IPA ambient, Figure 10b compares the simulated transfer characteristics (I_{DS} as a function of V_{GS}) of the 58µm long nanowires with different densities of surface states with the measured sub-threshold characteristics of the nano-sensor block with 58µm long nanowires in different gas ambient. We are able to reproduce the measured polysilicon nanowires transfer characteristics at different gas ambient only by incorporating donor type states. The measured sub-threshold characteristics in air is reproduced with donor type states in the top oxide/silicon interface for a density of $3\times10^{11}/cm^2$ which is similar to the density of $1.6\times10^{11}/cm^2$ that was used to reproduce the measured sub-threshold characteristics of 14 micron long nanowire in air (Figure 4b and 10a) giving us confidence that the surface states of the fabricated polysilicon nanowires is around ~$10^{11}/cm^2$ excluding defect states contribution from grain boundaries. The sub-threshold characteristics in vacuum and H_2 gases with pressures of 0.5, 1.0 and 1.5 bars are reproduced with donor type states with densities of $8\times10^{10}/cm^2$, $1.3\times10^{11}/cm^2$, $2.2\times10^{11}/cm^2$, $10^{12}/cm^2$ respectively. This result shows that $2.2\times10^{11}/cm^2$ number of states is annihilated when the ambient is changed from air into vacuum whereas $5\times10^{10}/cm^2$, $1.4\times10^{11}/cm^2$ and $9.2\times10^{11}/cm^2$ number of states are introduced when the ambient is switched from vacuum into H_2 gases with pressures of 0.5, 1.0 and 1.5 bar respectively. The simulation result for NW characteristics in IPA gas is quite interesting. The characteristics in IPA is reproduced with a donor type density of $1\times10^{8}/cm^2$ indicating that almost all of the surface states in air ($3\times10^{11}/cm^2$) is effectively removed when the NW is exposed into IPA vapour. This implies that the interaction of IPA vapour with NW surface cannot be explained by OH^- ion layer formation only. There is a complex mechanism of I_{PA} interaction with NWs that is reducing surface states and effectively working as passivation agent for NW surface states [41].

Reported studies suggest that gas sensing using conventional metal oxide film and nanoparticle based sensors in room temperature usually exhibit slow response/recovery times due to inherent electron transfer mechanism and gas adsorption chemistry [42]. Silicon nanowire based gas sensors are currently in interests due to its promise for fast response in room temperature [42]. However, detection limit (gas sensitivity) and/or conductance change upon gas exposure, response/recovery times of silicon based sensors typically depend on material topology (i.e. pore diameter/pore density for porous silicon and nanowire density for bottom up grown or chemically etched nanowires etc), nanowire dimension (i.e. diameter), doping density, surface stoichiometry/texture etc. Although porous silicon is believed to facilitate gas adsorption through randomly distributed pores, typical response time of porous silicon thin film sensors for different gases are around the order of several minutes [43,44]. In order to achieve fast response utilizing high surface to volume ratio, silicon nanowires are recently researched as gas sensors and response/recovery times are reduced to a value around 25 to 60 seconds for some gases [45,46]. Targeted analyte in gas phase and it's concentration also have significant effect on sensing due to gas adsorption/de-adsorption rate and time and hence, technology standpoint of our nano-sensors need to be compared with silicon based H_2 and polar volatile organic compound (i.e. IPA) sensors for same concentration of H_2 gas and IPA vapour. Table 3 compares the gas sensing figure of merit (i.e. , response/recovery times and conductance change) of our polysilicon nanowire sensors with the only few reported silicon based gas sensors for H_2 and polar volatile organic compound (i.e. IPA). In this comparison we only consider pristine silicon material without any surface modifications to judge the intrinsic capability of our nano-sensor to detect H_2 and IPA molecules in gas phase. As can be seen from the table our polysilicon nanowire sensors exhibit much better response/recovery times in comparison to reported silicon based H_2/polar volatile organic compound sensors and

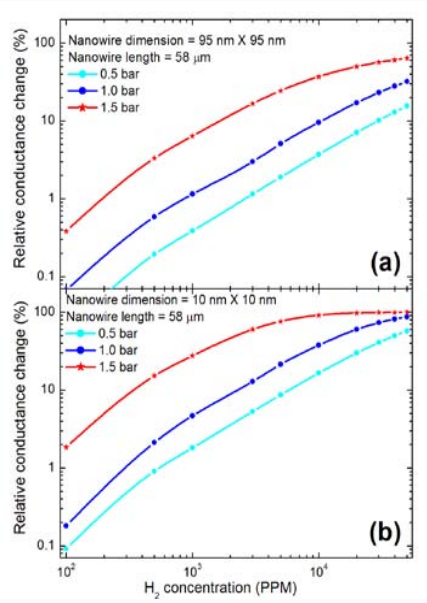

Figure 11: Polysilicon nanowire's peak conductance change (%) with respect to air as a function of H_2 gas concentrations for a) 95nm × 95nm and b) 10nm × 10nm polysilicon nanowire at different pressures. The nano-sensor block has 58μm long nanowires and 30 nanowires connected in parallel.

demonstrate appreciable conductance change for H_2/IPA sensing for the same concentration of H_2 (5%) and for the same environment of I_{PA} exposure (μl drop of the solvent to a tissue above a hole in a measurement box).

For safety applications gas sensors should be capable of detecting targeted analytes below their lower explosive limits (LEL) which are 4% (40,000ppm) and 2.2% (22,000ppm) for H_2 gas and I_{PA} vapour respectively. To investigate the detection limit of the fabricated polysilicon nanowires towards H_2 gas and IPA vapour, 3D simulation of electrical characteristics is performed for 58μm long polysilicon nanowire by incorporating surface states densities corresponding to different concentrations of H_2 gases and relative conductance change is calculated. Figure 10b exhibited that $5\times10^{10}/cm^2$, $1.4\times10^{11}/cm^2$ and $9.2\times10^{11}/cm^2$ number of states were introduced when polysilicon nanowires were exposed to 5% H_2 gases with pressures of 0.5, 1.0 and 1.5 bar respectively. These information allowed us to incorporate relevant concentrations of surface states corresponding to different concentration of H_2 gas exposure at nanowire surface acknowledging the fact that incorporation of H_2 gas in the defect states of a thin SiO_2 layer on Si is predominantly reaction-controlled rather than diffusion limited [49]. Figure 11a shows the nanowire's peak conductance change (%) with respect to air as a function of H_2 gas concentrations for 58μm long, 95nm × 95nm polysilicon nanowire at different pressures. It can be seen that nanowire response (i. e. relative conductance change) increases with increasing H_2 concentrations and for a same concentration of H_2 flow, increase in pressure makes nanowire more responsive. Relative conductance change is the representative figure of merit that sets the gas sensitivity of sensor. The nano-sensor block tested for gas sensing comprised 58μm long nanowires and 30 nanowires connected in parallel had a base current of 1.3nA at V_{GS}=-0.75 V (peak conductance change point) and 1% conductance change corresponds to a 13pA change in current. Agilent B1500A Semiconductor Parameter Analyser used for characterising electrical response of our nanowires at different ambient are capable of detecting even fA level of current. This can be set in differential mode where sensor response with targeted gas exposure is compared with sensor response in air to display the relative change in current and, hence we set 1% relative conductance change as our lowest detection limit. Figure 11a shows that the setting of 1% conductance change as a viable detection limit allows the nanosensor block detecting 2500ppm, 900ppm and 200ppm of H_2 gases at pressures of 0.5, 1.0 and 1.5 bar respectively. The presented technology should be scalable by depositing very thin α-Si layer followed by spacer etch and hence, Figure 11b shows the nanowire's peak conductance change (%) with respect to air as a function of H_2 gas concentrations for 58μm long, 10nm × 10nm polysilicon nanowire at different pressures. It can be observed that 10nm × 10nm polysilicon nanowire is capable of detecting 550ppm and 280ppm of H_2 gases at pressures of 0.5 bar and 1 bar respectively. For a slightly elevated pressure than atmospheric one (i.e. 1.5 bar) this sensitivity even goes below 100ppm. Elemental gases (i.e. H_2) have very low sticking coefficient on silicon surfaces whereas polar gas molecules like IPA has high sticking coefficient [50] and, hence it can be safely stated that IPA gas sensitivity limit of our polysicon nanowires is significantly superior that H_2 gas.

The aforementioned discussions unambiguously demonstrate potential of our polysilicon nanowire technology for H_2 and IPA gas sensing. In integrated sensor system, the sensing element is part of a large electronic circuit where sensor response in targeted gas is compared with reference response in air that is coupled with differential amplification scheme to convert a hardly detectable change in current to a detectable signal and hence, the sensitivity limit the polysilicon nanowires can be further improved in sensor system with integrated electronics. Using revolutionary advancement of nanotechnology the sensor/reference chamber can also be coupled with nano electromechanical system (NEMS) to control pressure or to create vacuum. In this regard, our polysilicon nanowire's gas sensitivity in vacuum may have interest and hence, polysilicon nanowire sensor's response with respect to vacuum has also been investigated and presented in the supplementary information section. In such an arrangement, 95nm × 95nm polysilicon nanowire will be able to detect 315ppm and 180ppm of H_2 gases at pressures of 0.5 bar and 1 bar whereas 10nm × 10nm polysilicon nanowire will be able to detect 240ppm and 130ppm of H_2 gases at pressures of 0.5 bar and 1 bar respectively. At H_2 gas pressure of 1.5 bar this sensitivity will be phenomenological which is significantly lower than 100ppm. The seminal review papers by Wan et al [51] and Smet et al [8] on semiconducting nanowire gas sensors show that pristine silicon nanowires demonstrate no appreciable sensor performance in H_2 and hence, decoration of silicon nanowires with H_2-sensitive pd nanoparticles is attempted. It is found that such a strategy is quite successful in converting silicon based platform selective and responsive for H_2 gas and silicon nanowires provide improved response/recovery times around 15-20 seconds [52]. Similar to H_2 sensing, Hossam Haick [53] used chemical functionalization of silicon nanowire for selective polar VOC sensing and also found better response/recovery times around 10-20 seconds in chemically modified nanowires in comparison to the reported bare silicon nanowire [45]. While suitable surface modification scheme can convert a typically irresponsive silicon nanowire sensor responsive and selective for gas sensing with a significant improvement in response recovery time, our inherently responsive polysilicon nanowire sensors with impressive response/recovery time obviously shows route towards promising sensors for detecting molecules in gas phase by adopting suitable surface

modification scheme and the platform has obvious advantage over single crystal silicon nanowires in terms of cost, manufacturability could open up opportunities in low cost disposable diagnostics and in portable, wearable or even implantable sensors.

Conclusions

We have presented a uniform and reproducible thin film polycrystalline silicon nanowire sensor technology by a rigorous investigation of the effect of spacer etch on the nanowire dimension, shape and have demonstrated room temperature gas detection using polysilicon nanowires. Perfectly rectangular and reasonably uniform polycrystalline silicon nanowires have been defined by spacer etch using low density plasma of SF_6/O_2gases from thin α-Si layer in a low cost reactive ion etch (RIE) equipment and well established 3 micron lithography which delivered promising control of the nanowire width and shape across a 6 inch wafer. The realized nano-sensors' conductance scaling with nanowire numbers and nanowire lengths are found to be in reasonable agreement with the design. The conductance variation of randomly distributed nano-sensors in a 6 inch wafer is found to be less than 7% implying a well controlled fabrication process for nano-sensors. Comparative measurements in air, vacuum, hydrogen and isopropyl alcohol have demonstrated the potential of polysilicon nanowires as gas sensors in room temperature with remarkable gas sensitivity and impressive response/recovery times that are noticeably better than reported pristine silicon based nano-sensors. 3D numerical simulations of polysilicon nanowires have indicted the evolution of surface states in different gas ambient which is the testament of gas sensing ability of the polysilicon nanowires. The developed thin film polysilicon nanowire sensors show route towards simple, low cost, mass manufacturable nano-sensor fabrication which is compatible with glass or plastic substrates could open up opportunities in low cost disposable diagnostics and in portable, wearable or even implantable sensors.

Acknowledgements

The authors would like to acknowledge the support of the Engineering and Physical Sciences Research Council (EPSRC), UK and the Center for Research & Training (CRT), East West University, Dhaka-1212, Bangladesh for funding this research Special thanks to clean room engineers of Southampton Nano-fabrication Center for assisting the fabrication/characterisation of nano-sensor chips and East West University Simulation Lab for providing TCAD simulation facility of nano-sensors.

References

1. Y Cui, Q Wei, H Park and CM Lieber. Nanowire nanosensors for highly sensitive and selective detection of biological and chemical species. Science. 2007; 293: 1289-1292.
2. F Patolsky, G Zheng and CM Lieber. Nanowire-based Biosensors. Anal. Chem. 2006; 78: 4260-4269.
3. H Ogi, K Motohisa, K Hatanaka, T Ohmori, M Hirao and M Nishiyama. High-Frequency Wireless and Electrodeless Quartz Crystal Microbalance Developed as Immunosensor. Jpn. J. Appl. Phys. 2007; 46: 4693-4697.
4. G Zheng, F Patolsky, Y Cui, WU Wang and CM Lieber. Multiplexed electrical detection of cancer markers with nanowire sensor arrays. Nat. Biotechnol. 2005; 23: 1294-1301.
5. Y Zhang and A Heller. Reduction of the Nonspecific Binding of a Target Antibody and of Its Enzyme-Labeled Detection Probe Enabling Electrochemical Immunoassay of an Antibody through the 7pg/mL–100ng/mL (40fM–400pM) Range. Anal. Chem. 2005; 77: 7758-7762.
6. MC McAlpine, RS Friedman, S Jin, KH Lin, WU Wang and CM Lieber. High-Performance Nanowire Electronics and Photonics on Glass and Plastic Substrates. Nano Lett. 2003; 3: 1531-1535.
7. E Stern, JF Klemic, DA Routenberg, PN Wyrembak, DB Turner-Evans, AD Hamilton, et al. Label-free immunodetection with CMOS-compatible semiconducting nanowires. Nature. 2007; 445: 519-522.
8. A Cao, Ernst JR Sudhölter and CPM Smet. Silicon Nanowire-Based Devices for Gas-Phase Sensing. Sensors. 2014; 14: 245-271.
9. W Lu, P Xie and CM Lieber. Nanowire Transistor Performance Limits and Applications. IEEE Trans. on Elecron. Dev. 2008; 55: 2859-2876.
10. ZQ Gao, A Agarwal, AD Trigg, N Singh, C Fang, CH Tung, et al. Silicon Nanowire Arrays for Ultrasensitive Label-Free Detection of DNA. Anal. Chem. 2007; 79: 3291-3297.
11. I Park Z Li, AP Pisano and RS Williams. Top-down fabricated silicon nanowire sensors for real-time chemical detection. Naotechnology. 2010; 21: 015501.
12. YL Bunivomich, YS Shin, WS Yeo, M Amori, G Kwong and JR Heath. Quantitative Real-Time Measurements of DNA Hybridization with Alkylated Nonoxidized Silicon Nanowires in Electrolyte Solution. J. Am. Chem. Soc. 2006; 128: 16323-16331.
13. NA Melosh, A Boukai, F Diana, B Geradot, A Badolato, PM Petroff, et al. Ultrahigh- density nanowire lattices and circuits Science. 2003; 300: 112-115.
14. GJ Zhang, JH Chua, RE Chee, A Agarwal and SM Wong. Label-free direct detection of MiRNAs with silicon nanowire biosensors. Biosensors and Bioelectronics. 2009; 24: 2504-2508.
15. S Chen, JG Bomer, WG Van der Wiel, ET Carlen and A Van den Berg. Top-down fabrication of sub-30 nm monocrystalline silicon nanowires using conventional microfabrication. ACS Nano. 2009; 3: 3485-3492.
16. MH Lee, KN Lee, SW Jung, WH Kim, KS Shin and WK Seong. Quantitative measurements of C-reactive protein using silicon nanowire arrays. International Journal of Nanomedicine. 2008; 3: 117-124.
17. F Patlosky, G Zheng and CM Lieber. Fabrication of silicon nanowire devices for ultrasensitive, label-free, real-time detection of biological and chemical species. Nat. Protoc. 2006; 1: 1711-1724.
18. CY Hsiao, CH Lin, CH Hung, CJ Su, YR Lo, CC Lee, et al. Novel poly-silicon nanowire field effect transistor for biosensing application. Biosensors and Bioelectronics. 2009; 24: 1223-1229.
19. Ming-Pei Lu, Cheng-Yun Hsiao, Wen-Tsan Lai and Yuh-Shyong Yang. Probing the sensitivity of nanowire-based biosensors using liquid-gating. Nanotechnology. 2010; 21: 425505.
20. C-H Lin, C-Y Hsiao, C-H Hung, Y-R Lo, C-C Lee, C-J Su, et al. Ultrasensitive detection of dopamine using a polysilicon nanowire field-effect transistor. Chem. Commun. 2008; 44: 5749-5751.
21. HC Lin, MH Lee, CJ Su, TY Huang, CC Lee and YS Yang. A simple and low-cost method to fabricate TFTs with poly-si nanowire channel. IEEE Electron Device Lett. 2005; 26: 643-645.
22. CJ Su, HC Lin, HH Tsai, TM Wang, TY Huang and WX Ni. Operations of poly-Si nanowire thin-film transistors with a multiple-gated configuration. Nanotechnology. 2007; 18: 215205.
23. IC Chen, CW Teng, DJ Coleman and A Nishimura. Interface-Trap Enhanced Gate-Induced Leakage Current in MOSFET. IEEE Electron Dev. Lett. 1989; 10: 216-218.
24. MMA Hakim, L Tan, O Buiu, WR White, S Hall and P Ashburn. Improved sub-threshold slope in short channel vertical MOSFETs using FILOX oxidation. Solid State Electronics. 2009; 53: 753-759.
25. Mohammad MA Hakim, Marta Lombardini, Kai Sun, Francesco Giustiniano, Peter L Roach, Donna E Davies, et al. Thin Film Poly-

crystalline Silicon Nanowire Biosensors. Nano Letters. 2012; 12: 1868-1872.

26. L Kenoyer, R Oxford and A Moll. Optimization of Bosch etch process for through wafer interconnects. Proceedings of the 15th Biennial University/Government/Industry Microelectronics Symposium, Boise, ID, USA. 2003: 338-339.

27. JK Bhardwaj and H Ashraf. Advanced silicon etching using high-density plasmas. SPIE Micromachining and Microfabrication Process Technology. 1995; 2639: 224-233.

28. TY Huang, IW Wu and JY Chen. Use of sacrificial spacers for fabricating LDD transistors in a CMOS process. Electronic Letters. 1986; 22: 430-432.

29. MD Henry. California Institute of Technology, USA. 2010.

30. Robert Bosch (Gmbh), U. S. Patent 4855017, (September 08, 1988).

31. C Chang, YF Wang, Y Kanamori, JJ Shih, Y Kawai, CK Lee, et al. Etching submicrometer trenches by using the Bosch process and its application to the fabrication of antireflection structures. J. of Micromech. And Microeng. 2005; 15: 580-585.

32. Jiansheng Jie, Wenjun Zhang, Kuiqing Peng, Guodong Yuan, Chun Sing Lee, and Shuit-Tong Lee. Surface-Dominated Transport Properties of Silicon Nanowires. Advanced Functional Materials. 2008; 18: 3251-3257.

33. Ping Xie, Yongjie Hu, Ying Fang, Jinlin Huang and Charles M Lieber. Diameter-dependent dopant location in silicon and germanium nanowires. PNAS. 2009; 106: 15254-15258.

34. Chung-Hoon Lee, Clark S Ritz, Minghuang Huang, Michael W Ziwisky, Robert J Blise and Max G Lagally. Integrated freestanding single-crystal silicon nanowires: conductivity and surface treatment. Nanotechnology. 2011; 22: 055704.

35. Shelley A Scott, Weina Peng, Arnold M Kiefer, Hongquan Jiang, Irena Knezevic, Donald E Savage, et al. Influence of Surface Chemical Modification on Charge Transport Properties in Ultrathin Silicon Membranes. ACS Nano. 2009; 7: 1683-1692.

36. JS Jie, WJ Zhang, Y Jiang, XM Meng, YQ Li, ST Lee. Photoconductive Characteristics of Single-Crystal CdS Nanoribbons. Nano Letters. 2006; 6: 1887-1892.

37. D Wang, Y-L Chang, Q Wang, J Cao, DB Farmer, RG Gordon, et al. Surface chemistry and electrical properties of germanium nanowires. J. Am. Chem. Soc. 2004; 126: 11602-11611.

38. Hideo Fujii, Seigo Kanemaru, Takashi Matsukawa, and Junji Itoh. Air-bridge-structured silicon nanowire and anomalous conductivity. Applied Physics Letters. 1999; 75: 3986-3988.

39. P Walker, H Mizuta, S Uno, Y Furuta and D Hasko. Improved off-current and subthreshold slope in aggressively scaled poly-Si TFTs with a single grain boundary in the channel. IEEE Trans. On. Electron Devices. 2004; 51: 212-219.

40. RH Kingston. Semiconductor Surface Physics. University of Pennsylvania Press, Philadelphia, PA. 1957.

41. JKl-Demellawi, CR Holt, E Abou-Hamad, ZA Al-Talla, Y Saih and S Chaieb. Room-Temperature Reactivity Of Silicon Nanocrystals With Solvents: The Case Of Ketone And Hydrogen Production From Secondary Alcohols: Catalysis? Applied Materials & Interface. 2015; 7: 13794-13800.

42. Rakesh K Joshi and Ashok Kumar. Room temperature gas detection using silicon nanowires. Materials Today. 2011; 14: 522011.

43. Stephen Lewis. Georgia Institute of Technology. USA. 2006.

44. C Baratto, G Sberveglieri, E Comini, G Faglia, G Benussi, V La Ferrara, et al. Gold-catalysed porous silicon for NOx sensing. Sensors and Actuators B. 2000; 68: 74-80.

45. O Niskanen, A Colli, R White, HW Li, E Spigone and JM Kivioja. Silicon nanowire arrays as learning chemical vapour classifiers. Nanotechnology. 2011; 22: 295502.

46. Kui-Qing Peng, Xin Wang and Shuit-Tong Lee. Gas sensing properties of single crystalline porous silicon nanowires. Applied Physics Letters. 2009; 95: 243112.

47. NK Ali, MR Hashim, A Abdul Aziz. Effects of surface passivation in porous silicon as H_2 gas sensor. Soild-State Electronics. 2008; 52: 1071-1074.

48. Hangbo Zhao. Massachusetts Institute of Technology, USA. 2014.

49. F Messina and M Cannas. Character of the Reaction between Molecular Hydrogen and a Silicon Dangling Bond in Amorphous SiO_2. J. Phys. Chem. C. 2007; 111: 6663-6667.

50. M Dürr and U Höfer. Dissociative adsorption of molecular hydrogen on silicon surfaces. Surface Science Reports. 2006; 61: 465-526.

51. P Feng, F Shao, Y Shi and Q Wan. Gas Sensors Based on Semiconducting Nanowire Field-Effect Transistors. Sensors. 2014; 14: 17406-17429.

52. Jae-Hyuk Ahn, Jeonghoon Yun, Dong-Il Moon, Yang-Kyu Choi and Inkyu Park. Self-heated silicon nanowires for high performance hydrogen gas detection. Nanotechnology. 2015; 26: 095501.

53. Bin Wang and Hossam Haick. Effect of chain length on the sensing of volatile organic compounds by means of silicon nanowires. Applied Materials & Interfaces. 2013; 5: 5748-5756.